Decadal Buoyancy Forcing in a Simple Model of the Subtropical Gyre

A. CZAJA AND C. FRANKIGNOUL

Laboratoire d'Océanographie Dynamique et de Climatologie, Unité Mixte de Recherche, CNRS–ORSTOM–UPMC, Université Pierre et Marie Curie, Paris, France

(Manuscript received 27 October 1998, in final form 1 March 1999)

ABSTRACT

The decadal response of the ventilated thermocline to surface buoyancy forcing is investigated, using simplified mixed layer thermodynamics and two-layer planetary geostrophic dynamics. The model is forced by a stationary Ekman pumping and a fluctuating sea surface density, while the associated surface buoyancy flux is diagnosed from the buoyancy budget of ventilated columns. The decadal forcing is represented as a slow modulation of the seasonal cycle, rather than a slow periodic forcing as in Liu and Pedlosky. It is found that the amplitude and the degree of nonlinearity of the interior response depend on the anomalies of the yearly averaged surface buoyancy flux, but that omitting the seasonal cycle leads to an overestimation of the thermocline variability by a factor of 2. At periods longer than 10 years, the interior response becomes linear and frequency independent so that in the presence of stochastic buoyancy forcing the spectrum of potential vorticity or interface displacement is white at low frequency and red at high frequency. A statistical signature of the buoyancy forcing is the asymmetric shape of the cross-covariance function between sea surface density and interface displacement anomalies in lead and lag conditions.

1. Introduction

In his seminal study of the ventilation of the subtropical gyre, Stommel (1979) discussed how the seasonally varying properties of the surface mixed layer affect the ocean interior, and showed that only water subducting in early spring could penetrate the permanent thermocline and avoid being reentrained in the mixed layer during the following fall and winter. This selection process, known as Stommel's demon, was shown to operate in the North Atlantic subtropical gyre in the observations (Marshall et al. 1993) and numerical models (Williams et al. 1995), with an effective subduction period of about one month. Year-to-year variations of mixed layer properties at the end of winter are thus likely to produce changes in the ventilated interior. Deser et al. (1996), indeed, suggested that the decade-long cooling and deepening of the mixed layer that was observed in the 1980s in the central North Pacific would penetrate to greater depth trough ventilation, while Miller et al. (1994) had shown that, if surface heat flux and wind anomalies were responsible for the surface cooling, the subduction of the thermal anomalies would be consistent with the mean currents. In a similar way, New and Bleck (1995) proposed that a large part of the low-frequency variability observed in the first 1000 m of the North Atlantic by Levitus (1989) could result from the subduction of water from a colder mixed layer without requiring changes in Ekman pumping.

From a theoretical point of view, little attention has been given to the buoyancy forcing of the thermocline. Using a normal mode approach, Frankignoul and Müller (1979) suggested that stochastic forcing by buoyancy flux was much smaller than by Ekman pumping in the wavenumber–frequency range of geostrophic eddies, while Liu and Pedlosky (1994, hereafter LP), using a two-layer planetary geostrophic model, argued that, at decadal frequencies, buoyancy forcing would dominate wind forcing in the ventilated area. However, the large range of amplitude given to the prescribed displacement of the first layer outcrop line was not related to the sea surface density or surface buoyancy flux variations, so the relevance of their predictions to the observations was unclear. Moreover, since the seasonal cycle of the mixed layer was not represented, the physics of the interannual fluctuations of the mixed layer depth, which is representative of the year-to-year changes of the mixed layer depth at the end of winter, according to Stommel's demon, needs to be clarified. The aim of this paper is to estimate more quantitatively the thermocline response to low-frequency buoyancy forcing, using a crude but more realistic representation of the mixed layer that takes into account its seasonal cycle, which will be shown to reduce the interior variability by a factor of 2. The model is otherwise a straightforward extension

Corresponding author address: Dr. Arnaud Czaja, MIT Building 54, Room 1421, 77 Massachusetts Ave, Cambridge, MA 02139.
E-mail: czaja@ocean.mit.edu

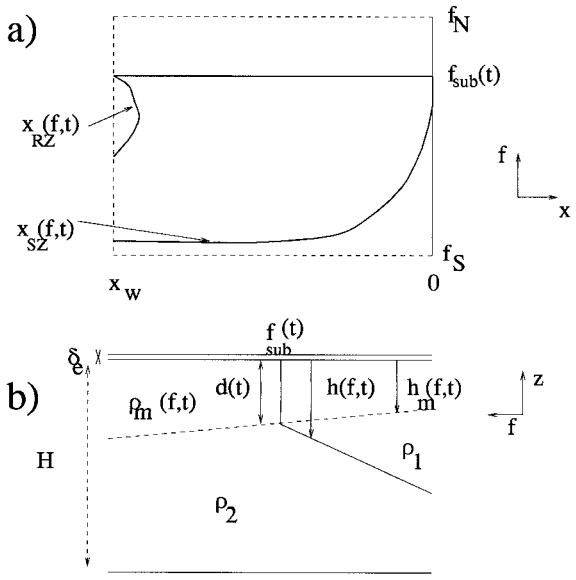

FIG. 1. (a) Horizontal extent of the model. (b) Latitude–depth section of the model. The thickness of the Ekman layer δ_e is taken infinitely thin.

of that of LP, and it is also forced by the fluctuations in the surface density rather than the buoyancy flux. However, the latter is diagnosed with a simple thermodynamic subduction model.

The structure of the paper is as follows: Section 2 presents the governing equations and the mixed layer model. Section 3 is devoted to the diagnostic of the surface buoyancy flux. The model response to a decadal modulation of the annual migration of the outcrop line is presented in section 4, and a stochastic forcing experiment in section 5. The main results are discussed in section 6.

2. A model of the ventilated subtropical gyre

a. The gyre model

The thermocline model consists of two adiabatic layers of constant density ρ_1 and ρ_2 below a surface mixed layer, whose density ρ_m and depth h_m are only functions of time and latitude, and which includes an infinitely thin Ekman layer at the top (Fig. 1). As in LP, the model has a free surface ξ and the depth H of the thermocline bottom is taken as a constant. The Coriolis parameter is used as meridional coordinate. The model subtropical gyre extends from x_W to 0, f_S to f_N, and the β-plane approximation is used. For such a two-layer model, a constant meridional gradient is best suited for both ρ_m and h_m. Defining $f_{\text{sub}}(t)$ as the f coordinate of the first layer outcrop line, we choose to satisfy $\rho_m(f, t) = \rho_1$ at $f = f_{\text{sub}}(t)$, which leads to

$$\rho_m(f, t) = \rho_1 + \mu_1[f - f_{\text{sub}}(t)] \tag{1}$$

$$h_m(f, t) = d(t) + \mu_2[f - f_{\text{sub}}(t)], \tag{2}$$

where μ_1 and μ_2 are the constant meridional gradients of density and depth of the mixed layer, and d its depth at the outcrop line, which is a model variable whose calculation is described below. Since d varies, h_m is not entirely specified in terms of f_{sub}, contrary to ρ_m. The buoyancy forcing is modeled by prescribing the outcrop line displacement, which is thus equivalent to specifying the surface density. Since μ_1 and μ_2 are positive, the mixed layer deepens (shoals) and cools (warms) when the outcrop line moves toward the south (north). The ratio of mixed layer density and depth changes is μ_1/μ_2. For the standard model parameters listed in Table 1, this corresponds to a 15-m depth variation for a 1°C sea surface temperature (SST) anomaly. Note that (1) and (2) are longitude independent and that the mixed layer depth and density fluctuations are also latitude independent.

To emphasize the buoyancy forcing effects, the Ekman pumping is time independent:

$$w_e = w_e(f) = 4w_0\frac{(f - f_N)(f - f_S)}{(f_N - f_S)^2} \tag{3}$$

with a maximum amplitude w_0 at $f = (f_N + f_S)/2 = f_M$. The zonal and meridional Ekman transports satisfy $w_e = \text{div}(\mathbf{V}_e)$ and are given by

$$\begin{cases} U_e = 0 \\ V_e = \dfrac{4w_0}{\beta(f_N - f_S)^2} \\ \qquad \times \left[\dfrac{(f - f_M)^3}{3} - f_M(f^2 - f_M^2) + f_N f_S(f - f_M)\right]. \end{cases} \tag{4}$$

Since f_{sub} and w_e are prescribed, the unknowns are the free surface ξ, the depth h of the interface between the two thermocline layers, and the mixed layer depth d at the outcrop line. The model differs from that of LP since 1) the moving outcrop line is explicitly related to the mixed layer depth and density, 2) the mixed layer depth d at the outcrop line is not prescribed but calculated, and 3) the Ekman pumping varies with latitude, allowing recirculation zones and a distinction between subpolar and subtropical gyres.

To derive the governing equation for the interface depth, first consider the dynamic pressures, given in each layer by the integration of the hydrostatic equation

$$\begin{cases} \dfrac{p_m}{\rho_0} = \gamma\eta + \gamma_m z \\ \dfrac{p_1}{\rho_0} = \gamma\eta - \gamma_m h_m \\ \dfrac{p_2}{\rho_0} = \gamma(\eta - h) - \gamma_m h_m, \end{cases} \tag{5}$$

where the reduced gravity between layers 1 and 2 and

TABLE 1. Standard model parameters.

Quantity	Variable	Value
Northern boundary coordinate	f_N	10^{-4} s^{-1} (f *at* 45°N)
Southern boundary coordinate	f_S	3.8×10^{-5} s^{-1} (f *at* 15°N)
Meridional gradient of planetary vorticity	β	2×10^{-11} m^{-1} s^{-1} (β *at* 30°N)
Depth of the thermocline bottom	H	600 m
Reduced gravity between layers 1 and 2	γ	10^{-2} m s^{-2}
First-layer density	ρ_1	1024.5 kg m^{-3}
Reference density	ρ_0	1000 kg m^{-3}
Thermal expansion coefficient of seawater	α_T	2.5×10^{-4} K^{-1}
Meridional gradient of the mixed layer density	μ_1	2.6×10^{4} s kg m^{-3}
Meridional gradient of the mixed layer depth	μ_2	1.5×10^{6} s m
Vertical gradient of density	Γ	0.01 kg m^{-4}
Shallowing parameter	k	0.32 m/W m^{-2}
Time interval	Δt	0.25 yr
Maximum Ekman pumping	w_0	45 m yr^{-1}
Subduction line displacement: seasonal amplitude	a	0.2
Subduction line displacement: decadal amplitude	b	0.04
Subduction line displacement: mean position	f_m	8.5×10^{-5} s^{-1} (f *at* 36°N)

between the mixed layer and layer 1 are denoted respectively by $\gamma = g(\rho_2 - \rho_1)/\rho_0$ and $\gamma_m = g(\rho_1 - \rho_m)/\rho_0$ (ρ_0 is the reference density), and the rescaled free surface η is defined by $\gamma\eta = g\xi$. Geostrophic balance in each layer yields

$$(u_\alpha, v_\alpha) = \frac{1}{f\rho_0}(-p_{\alpha y}, p_{\alpha x}) \quad \text{with } \alpha = m, 1, 2. \tag{6}$$

Defining the barotropic pressure p_B from

$$H\mathbf{v}_B = (H - h)\mathbf{v}_2 + (h - h_m)\mathbf{v}_1 + \int_{-h_m}^{0} \mathbf{v}_m \, dz$$

$$= \frac{H}{\rho_0 f}\mathbf{k} \times \nabla p_B, \tag{7}$$

one obtains, after using (5) and (6),

$$\frac{p_B}{\rho_0} = \frac{1}{2H}[\gamma_m h_m^2 + \gamma(H - h)^2 + 2H(\gamma\eta - \gamma_m h_m)]. \tag{8}$$

Assuming that the barotropic circulation is in Sverdrup equilibrium

$$(H - h)v_2 + (h - h_m)v_1 + \int_{-h_m}^{0} v_m \, dz = \frac{fw_e}{\beta} \tag{9}$$

and integrating (9) along the x axis with a zero barotropic transport at the eastern boundary, one gets

$$\frac{p_B}{\rho_0} = \frac{f^2 w_e x}{\beta H}. \tag{10}$$

Equations (8) and (10) enable one to express η in terms of h and (γ_m, h_m). The evolution equation for h is the conservation of the lower-layer potential vorticity $q = f/(H - h)$ (hereafter PV) south of the outcrop line

$$\frac{\partial q}{\partial t} + u_2\frac{\partial q}{\partial x} + \beta v_2\frac{\partial q}{\partial f} = 0 \quad \text{for } f \le f_{\text{sub}}(t). \tag{11}$$

This equation can be written in characteristic form, which determines the different dynamical regions of the gyre. Here we concentrate on the ventilated zone, where the lower-layer columns originate from the outcrop line. This region is bounded by a shadow zone, for which the characteristics of (11) emanate from the eastern boundary, and a recirculation zone for which they emanate from the western boundary. The boundaries between the three dynamical regions (Fig. 1a) are denoted by $x_{SZ}(f, t)$ and $x_{RZ}(f, t)$ and their calculation is left to the appendix, where h is shown to be independent of x in the ventilated region. Then, from (5), (6), and (8) the meridional velocity in all layers is equal to the barotropic meridional velocity v_B:

$$v_1 = v_2 = v_m = v_B$$

$$= \frac{fw_e}{\beta H} \quad \text{for} \begin{cases} f \le f_{\text{sub}}(t) \\ x_{RZ}(f, t) \le x \le x_{VZ}(f, t). \end{cases} \tag{12}$$

A similar relation holds north of the outcrop line [use (5), (6) and (8) with $h = h_m$]:

$$v_2 = v_m = v_B \quad \text{for } f \ge f_{\text{sub}}(t). \tag{13}$$

Because of the flat thermocline bottom and the x independence of the mixed layer depth and density, the lower-layer PV at the outcrop line or subducted PV, $q_{\text{sub}} = f_{\text{sub}}/(H - d)$, is only a function of time. From (12), the lower-layer meridional velocity is, as w_e, x independent. Hence, meridional advection does not lead to any zonal variations of PV in the ventilated zone. Equation (11) simplifies to

$$\frac{\partial h}{\partial t} + \frac{fw_e}{H}\frac{\partial h}{\partial f} = -\left(1 - \frac{h}{H}\right)w_e \quad \text{for } f \le f_{\text{sub}}(t) \tag{14}$$

with the moving boundary condition

$$h(f, t) = d(t) \quad \text{at } f = f_{\text{sub}}(t). \tag{15}$$

The interior dynamics has been greatly simplified. The response to Ekman pumping consists in a local deep-

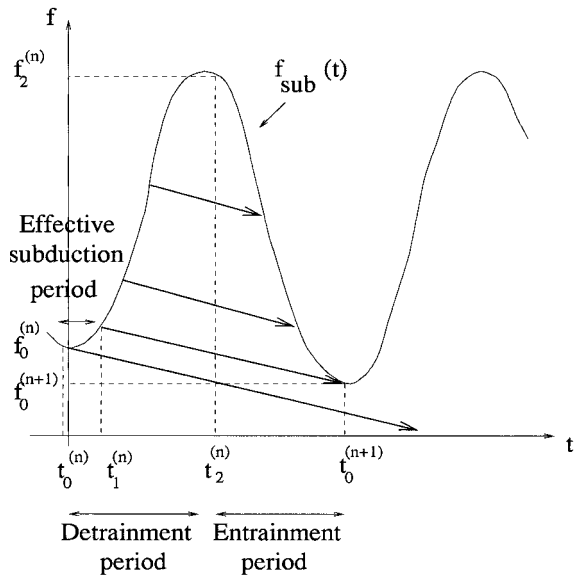

FIG. 2. Schematic of the outcrop line displacement (24), shown as a cosinelike curve, and associated time and f coordinate. In the course of year n, the latitude reached by columns subducting during the detrainment period $[t_0^{(n)}, t_2^{(n)}]$ is indicated by the arrows. Only columns subducted before $t_1^{(n)}$ reach the permanent thermocline. Note the variable position of the outcrop line from one winter to the next.

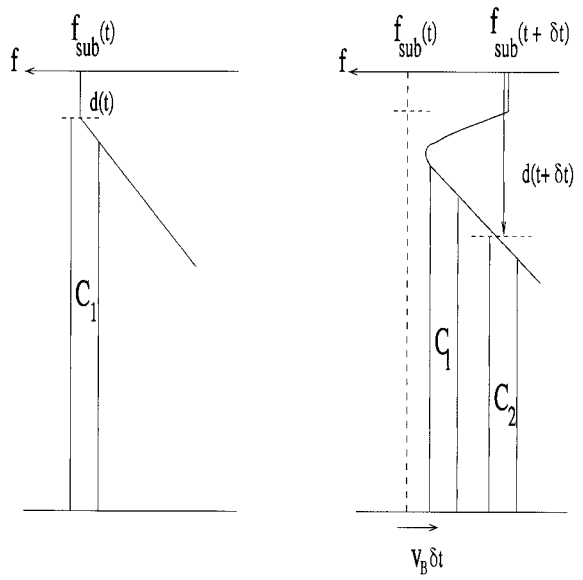

FIG. 3. Illustration of the convective adjustment scheme. At time $t + \delta t$ (right) the column C1 that has subducted at time t (left) reaches a higher latitude than the outcrop line, which generates a gravitationnal instability. This deepens the mixed layer to the top of column C2, which was previously subducted.

ening of the interface and a southward advection by the Sverdrup flow. There is no Rossby wave in the ventilated area because there is no x dependence.

b. The mixed layer model

Northern Hemisphere observations show a large seasonal displacement of the outcrop lines (Levitus 1982), which reach their southernmost latitude by the end of winter, and their northernmost one by the end of summer. In the North Atlantic, they present a NW–SE tilt, and have a complex annual migration, while they remain more zonal in the North Pacific so that (1) fits better. For simplicity, following LP we model the annual migration of the outcrop by a harmonic oscillation,

$$f_{\text{sub}}(t) = f_m[1 - a\cos(2\pi t)], \tag{16}$$

where time has been normalized by a year, and its origin is taken as the first of March. In the model, only outcrops located south of 30°N in winter always belong to the subtropical gyre, while the others penetrate in the subpolar gyre during summer. A typical value for a in midlatitudes is 0.2, and for illustration, f_m has been set to the value of f at 36°N, in order to keep for simplicity the outcrop line in the subtropical gyre (between 28° and 44°N).

As shown by LP, the computation of d is constrained by the prescribed displacement of the outcrop line. For stability, d must decrease when the speed of the outcrop line exceeds the barotropic meridional velocity (detrainment period) and increase otherwise (entrainment period). Subduction only occurs during detrainment between times t_0 and t_2, satisfying

$$\frac{df_{\text{sub}}}{dt} - \beta v_B(f_{\text{sub}}) = 0 \quad \text{at } t = t_0, t_2. \tag{17}$$

This is schematically depicted in Fig. 2 for a general case with a slow modulation of the seasonal cycle (section 4). For the parameter values listed in Table 1, subduction occurs between 28 February and 2 September, but only water columns subducted before mid April (time t_1) penetrate permanently into the interior, the others being reentrained in the mixed layer during the following entrainment period $[t_2; t_0 + 1]$ (Fig. 2). The effective subduction period $[t_0; t_1]$ lasts about one month, in agreement with Stommel's demon.

The computation of d is based on the buoyancy budget of the mixed layer during the detrainment period, and on the convective adjustment scheme of LP during the entrainment one (Fig. 3). During detrainment, the local variation of the mixed layer buoyancy is only due to advective or surface inputs. Since the mixed layer buoyancy is longitude independent, this can be written below the Ekman layer, using (12):

$$h_m\frac{\partial \gamma_m}{\partial t} + \beta h_m v_B\frac{\partial \gamma_m}{\partial f} = B_{in} - B_e, \tag{18}$$

where B_{in} is the surface buoyancy flux and $B_e = -\beta V_e \mu_1 g/\rho_0$ the Ekman buoyancy transport. Following the outcrop line $f_{\text{sub}}(t)$ where $\rho_m = \rho_1$ and $h_m = d$, (18) can be written as

$$d(t)\left[\frac{df_{\text{sub}}}{dt} - \beta v_B(f_{\text{sub}})\right]\frac{\mu_1 g}{\rho_0} = B_{in}[f_{\text{sub}}(t), t] - B_e[f_{\text{sub}}(t)]$$
$$\text{for } t_0 \le t \le t_2. \quad (19)$$

The unknowns are $d(t)$ and $B_{in}[f_{\text{sub}}(t), t]$ so that we need a second relation to determine d. As a first step, we assume a linear relation during the first stage Δt of the restratification process

$$d(t) = d(t_0) - k[B_{in}[f_{\text{sub}}(t), t] - B_{in}(f_0, t_0)]$$
$$\text{for } t_0 \le t \le t_0 + \Delta t, \quad (20)$$

where $d(t_0)$ is any initial condition, $B_{in}(f_0, t_0) = -\beta\mu_1 V_e(f_0)g/\rho_0$ with $f_0 = f_{\text{sub}}(t_0)$ (Fig. 2) in view of (17) and (19), and k, Δt are given in Table 1. Equation (20) states that in early spring, the more the mixed layer gains buoyancy, the shallower it becomes. Then, we assume that d remains constant,

$$d(t) = d(t_0 + \Delta t) \quad \text{for } t_0 + \Delta t \le t \le t_2, \quad (21)$$

which together with (19) and (20) yields d during the detrainment period. Since a column subducted at time t_1 conserved its PV from t_1 to $t_0 + 1$, one has

$$\frac{f_{\text{sub}}(t_1)}{H - d(t_1)} = \frac{f_{\text{sub}}(t_0 + 1)}{H - d(t_0 + 1)}, \quad (22)$$

which yields the initial condition for d in the following year. The latter equation relates the mixed layer depth at the end of winter to that in early spring of the previous year. It is the key equation of the mixed layer model, which represents the complex physics of the entrainment period. As long as $\Delta t \ge t_1 - t_0$, the somewhat artificial assumption (21) has no influence on the mixed layer depth during the next winter. Furthermore, if the outcrop leaves the subtropical gyre at a time larger than t_1, the mixed layer model can also be applied from t_0 to t_1, which will be used in section 4.

The seasonal cycle is presented in Fig. 4, for the parameters listed in Table 1. It takes a few years for the mixed layer depth at the outcrop line to reach its end-of-winter equilibrium value of 125 m (not shown). Figure 4a shows the annual march of the outcrop line given by (16), which is associated with a moderate annual cycle of the surface density with $0.9\sigma_\theta$ peak to peak amplitude. From March to June, the mixed layer shoals by 40 m at the outcrop line (Fig. 4b), which corresponds to a shoaling of more than 70 m at a fixed latitude by (2). Since (19) only applies to the detrainment period, the surface buoyancy flux is only plotted for that period (Fig. 4c). During the effective subduction period (from the beginning of March to mid April), the outcrop line moves about 2 degrees northward and d shoals by 30 m. The shoaling is responsible for the initial decrease of the lower-layer PV at the outcrop line (Fig. 4c, dashed line) but, by the end of March, the vorticity gain induced by the surface buoyancy input dominates the PV evolution. Columns with high PV are reentrained in the mixed layer from September to February.

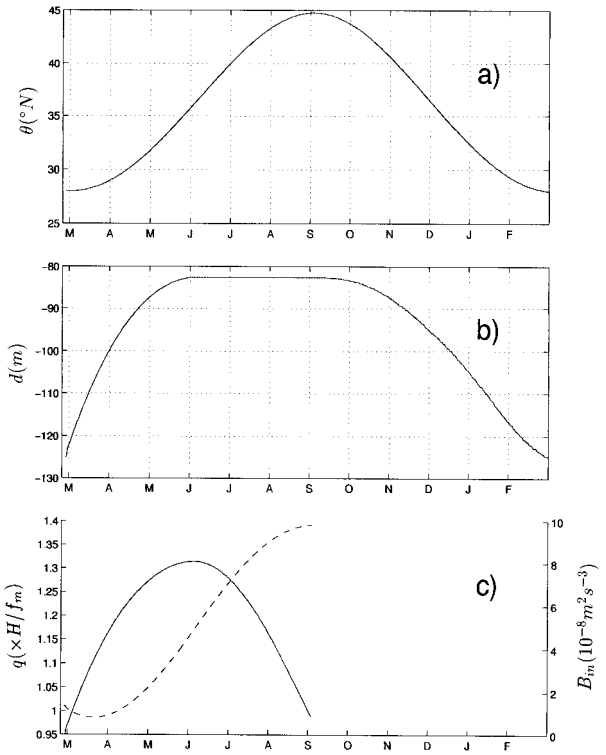

FIG. 4. (a) Outcrop line annual march, (b) mixed layer depth d at the outcrop line, and (c) surface buoyancy flux B_{in} (continuous line) and lower-layer PV (normalized by f_m/H, dashed line) at the outcrop line. The x axis denotes time, in months.

It should be emphasized that the mixed layer model does not require knowing the interface depth h, which can then be computed from (14) and (15). This is due to the assumption of a flat thermocline bottom and a zonal outcrop line. A tilted outcrop line would couple the ventilated interior to the mixed layer.

3. Diagnostic of the surface buoyancy flux

In section 2b, the surface buoyancy flux at the outcrop line was calculated by (19) during the detrainment period. Entrainment needs to be added in entrainment periods, but this is beyond the scope of our study. Nevertheless, the surface buoyancy flux can be diagnosed by considering the buoyancy content of a fluid column that extends below the mixed layer, in order for entrainment to merely redistribute buoyancy.

Consider a water column in the ventilated zone, extending throughout the mixed layer of depth $-h_0$ at $t = t_0$ (the first March) of a given year. For simplicity, we first assume that the column behaves barotropically during a one-year trajectory determined by the Sverdrup flow (u_B, v_B). From t_0 to $t_0 + 1$, the column moves to the south by Δf (about two degrees of latitude) and accordingly, its mixed layer depth shoals by $\mu_2 \Delta f$ (~10

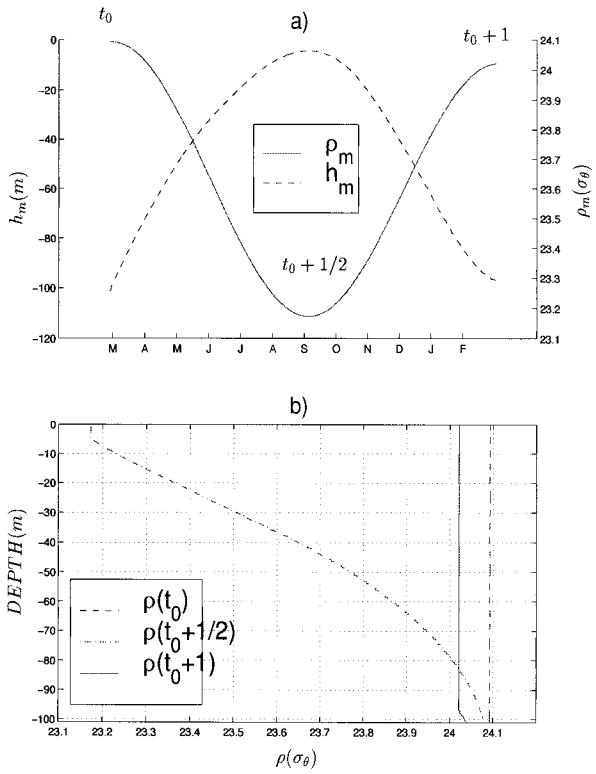

FIG. 5. (a) Evolution of the mixed layer depth (in m) and density (in σ_θ) along the 1-yr trajectory for the column initially located at 21.2°N. The x axis denotes time, in month. (b) Density profile at times t_0, $t_0 + ½$, and $t_0 + 1$.

m) and its density decreases by $\mu_1 \Delta f$ ($\sim 0.1\sigma_\theta$) (Fig. 5a). Along the course of the year, mixed layer water is added by Ekman pumping and injected into the interior by vertical advection. For simplicity, the vertical velocity is set to w_e throughout the column. Following Stommel (1979), the tracking of the water parcels provides a mean to compute the density profile in the interior. Consider a water parcel at depth z and time t. It has previously left the mixed layer at time $t_i(z, t)$ and latitude $f_i(t_i)$, which are easily determined by v_B. Since the mixed layer density was $\rho_m(t_i, f_i)$, we have $\rho(z, t) = \rho_m(t_i, f_i)$. The calculation is illustrated in Fig. 5b. From t_0 to $t_0 + ½$, the seasonal pycnocline has formed and the mixed layer shoaled by ~100 m. From one winter to the next, however, the former is eroded and only a small volume of stratified water escapes to be reentrained in the mixed layer.

TABLE 2. Various mean buoyancy fluxes deduced from the integration of (23) over time ($\Delta BC = \overline{B}_{in} + \overline{B}_v - \overline{B}_e$), for a column initially located at 21.2°N. All buoyancy fluxes are expressed in 10^{-8} $m^2\ s^{-3}$.

	Detrainment mean	Entrainment mean	Annual mean
$\overline{B}_v$	0.43	0.44	0.43
$\overline{B}_e$	−0.59	−0.63	−0.61
$\overline{B}_{in}$	1.45	−3.16	−0.82
ΔBC	2.47	−2.09	0.22

As shown by Marshall et al. (1993), the buoyancy content of the column beneath the Ekman layer is governed by the surface buoyancy flux B_{in}, the Ekman buoyancy transport $B_e = -(g/\rho_0)V_e d\rho_m/dy$, and the divergence of the vertical transport of buoyancy within the column $B_v = w_e(\rho_m - \rho_b)g/\rho_0$, where ρ_b denotes the density at the bottom of the column:

$$\left(\frac{\partial}{\partial t} + u_B\frac{\partial}{\partial x} + v_B\frac{\partial}{\partial y}\right)\int_{-h_0}^{0} -\left(g\frac{\rho}{\rho_0}\right)dz = B_{in} - B_e + B_v. \quad (23)$$

By the thermal wind relation, a meridional density gradient in the interior gives rise to a vertical shear of the zonal geostrophic velocity, which should be added to u_B in (23). However, since neither the mixed layer density nor the meridional velocity is x dependent, the subduction does not create any zonal density gradient in the interior on which the baroclinic flow could act. Hence our initial assumption of barotropic displacement does not affect the buoyancy budget of the column. Note that the baroclinic advection effect has been found to be negligible in a more general setting (e.g., Marshall et al. 1993; Paillet and Arhan 1996). Since B_e and B_v are easily derived from (3) and (4) using $\rho_b(t) = \rho(z, t)$ at $z = -h_0$, (23) provides a diagnostic relation between the buoyancy content of the column and its surface buoyancy flux, which can be integrated over the detrainment and the entrainment periods [approximated respectively as (t_0; $t_0 + ½$) and ($t_0 + ½$; $t_0 + 1$)], or during a whole year between t_0 and $t_0 + 1$. As summarized in Table 2 for the experiment in Fig. 5, the annual mean surface buoyancy flux is negative, as the buoyancy loss in the entrainment period is larger than the buoyancy gain in the detrainment one. In the latitude band covered by the chosen column, the annual Ekman buoyancy transport is not negligible but exceeds the buoyancy gain ΔBC between consecutive winters, like the annual divergence of vertical transport of buoyancy. In the latitude range of maximum Ekman pumping, the vertical divergence of buoyancy supplies most of the column annual buoyancy gain.

It should be emphasized that the rhs of (23) is taken following the column so that its averaging corresponds to a Lagrangian average over the few degrees of latitude covered by the column during the corresponding time interval. In periods of anomalous annual buoyancy loss, it may occur that the mixed layer depth at the end of the integration is larger than the initial column depth. In this case, the latter is set to the second winter mixed layer depth. The initial density profile of the column below the mixed layer is then simply assumed to be linear with a prescribed vertical gradient Γ.

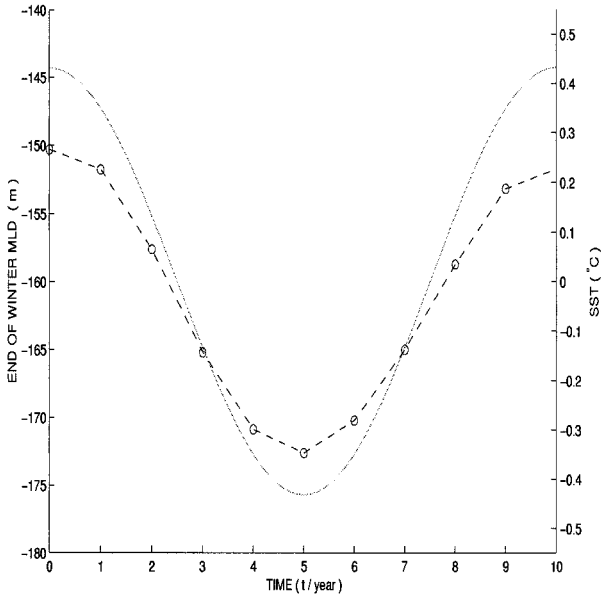

FIG. 6. Decadal modulation of the depth of the end-of-winter mixed layer at the outcrop line (in m, dashed line) and SST (in °C, continuous line).

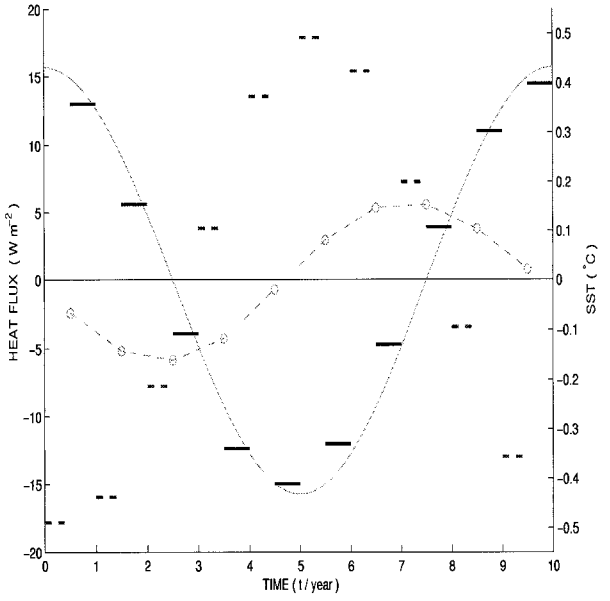

FIG. 7. Diagnostic of the surface heat flux for the latitude range 36–33.5°N. The SST modulation is shown by the continuous curve (in °C), and the annual heat flux anomaly (in W m^{-2}) by the the dashed line (the circles are centered on each year). The surface heat flux anomalies during entrainment (continuous line) and detrainment period (dashed line) are plotted as heavy horizontal bars.

4. Decadal buoyancy flux forcing

In section 2b, we showed that during the effective subduction period, the PV of subducting columns is determined in the model by the mixed layer shoaling (about 30 m) and the northward displacement of the outcrop line (about 2° of latitude). The observations show similar amplitudes at the decadal timescale, as in Deser et al.'s study (1996) where a SST anomaly of 0.75 K (peak to peak, corresponding to a 3° latitudinal displacement of the outcrops) is associated with a mixed-layer depth anomaly of 20 m: the ratio of mixed-layer depth change and outcrop displacement is only a factor 2 larger than predicted here for the seasonal cycle. It is therefore likely that, in concert with the interannual fluctuations of the outcrop line, the year-to-year variations of the mixed layer depth influence the PV of the columns subducting in the permanent thermocline. As the mixed layer depth should not only depend on the instantaneous forcing, but also on past conditions, it seems necessary to take into account the seasonal cycle of the mixed layer when representing the decadal forcing, even though it was neglected in LP. In the present paper, we consider that the outcrop line displacement is given by

$$f_{\text{sub}}(t) = f_m[1 - a\cos(\omega_{\text{yr}}t) + b\cos(\omega t)], \quad (24)$$

which for $\omega \ll \omega_{\text{yr}} = 2\pi/1$ yr represents a low-frequency modulation of the seasonal cycle.

a. Decadal modulation of the outcrop line annual march

In this section, we present the equilibrium response of our model for $\omega = 2\pi/10$ yr in (24). To estimate the amplitudes, we use SST observations since surface salinity fluctuations are poorly documented at low frequency. At the decadal timescale, peak to peak SST variations are $O(1\text{ K})$, about five times smaller than in the seasonal cycle, which yields $b \sim a/5 = 0.04$. The mean position of the end-of-winter outcrop line is taken at 35°N so that it may penetrate in the subpolar gyre in summer, but without influencing the permanent thermocline. The mean mixed layer depth d at the end of winter is taken as $d_0 = 160$ m and, correspondingly, in (20) one chooses $k = 0.15$ m/W m^{-2}. Otherwise, all parameters are as before. For simplicity, we discuss from now on the model forcing in terms of SST, and we prescribe the SST modulation to have an amplitude of 0.45°C. The heat flux is estimated diagnostically as in section 3.

Figure 6 shows that at the end of winter, the mixed layer depth at the outcrop line is out of phase with the prescribed SST modulation, with an amplitude of about 12.5 m, which, from (2), corresponds to local variations of 12.5 + 7.5 = 20 m. These anomalies are driven by fluctuations of the heat loss in the entrainment period reaching -15 W m^{-2} (Fig. 7). However, during detrainment, the anomalies are of similar amplitude but opposite sign, resulting in a small annual heat flux anomaly ($\sim$6 W m^{-2}). Because the mixed layer depth changes are small in winter ($\delta d/d_0 \sim 12.5/160 \ll 1$) and the wind is steady, the simple heat balance

$$d_0\frac{d\text{SST}'}{dt} = \frac{Q'_{\text{ann}}}{\rho_0 C_p} \quad (25)$$

is expected to hold, where the prime denotes an anomaly and $Q_{\rm ann}$ is the annual mean surface heat flux which varies with latitude as d_0. For $d_0 = 160$ m, (25) recovers an annual heat flux anomaly of 5.8 W m^{-2} in quadrature with the SST anomaly, in agreement with Fig. 7.

The lower-layer PV is mapped for April of each year of the decadal modulation in Fig. 8. The solution is only given for the ventilated zone, whose extension varies significantly from year to year. From years 0 to 4, the PV of the subducted columns is high, while it is low from years 5 to 9. These highs and lows are in phase with the modulation of the outcrop line, implying that planetary vorticity variations dominate the PV evolution of the permanently subducted columns. The role of the mixed-layer depth changes is emphasized in Fig. 9, which compares the lower-layer PV at the outcrop line during each of the ten effective subduction periods (gray line) with the PV evolution that would be predicted for a constant mixed layer depth (continuous line): the mixed-layer depth anomalies substantially reduce the PV variations since, during entrainment periods of anomalous heat gain (loss), the subducted columns have higher (lower) planetary vorticity but greater (smaller) thickness. The resulting variability in the permanent thermocline has a moderate amplitude (15 m at 32°N, Fig. 10) that decreases with latitude while being advected southward (the small bumps in Fig. 10 are associated with the yearly pulse of subduction). The maximum amplitude of the interface displacement Δh at latitude f is

$$\Delta h = f\left(\frac{1}{q_{\rm sub}^{\rm min}} - \frac{1}{q_{\rm sub}^{\rm max}}\right), \tag{26}$$

where $q_{\rm sub}^{\rm min}$ and $q_{\rm sub}^{\rm max}$ denote respectively the minimum and maximum value of $q_{\rm sub}$ in Fig. 9.

The variability of the interface depth is related to the surface heat flux as follows. The anomalous surface heat loss in the entrainment period of a given year determines the SST and mixed-layer depth anomalies, hence the PV anomalies of the columns leaving the mixed layer in late winter (the PV and SST anomalies have the same sign). As the latter are advected, they propagate the anomalous interface depth in the permanent thermocline, lower than normal h being associated with a previous surface heat gain. Figure 10 reveals an asymmetry between sharp rising and slow deepening of the interface, which, as discussed by LP, is linked to the nonlinearity of the thermocline response. Here we can relate this asymmetry to the annual surface heat flux anomalies. For instance at 31.3°N where the advective timescale is 2 years, a sharp rise of the interface is found between years 2 and 6 because of an anomalous annual surface heat loss two years earlier (Fig. 7). Since the annual heating anomalies decrease as the period of the forcing increases [see (25)], however, the thermocline response is expected to become linear at low frequency.

b. Comparison with LP

Liu and Pedlosky considered a harmonic oscillation of the outcrop line

$$f_{\rm sub}(t) = f_m[1 + b\cos(\omega t)] \tag{27}$$

and interpreted the thermocline response to frequencies lower than annual as that to interannually varying end-of-winter mixed layer properties. The solution was periodic with the period of the forcing. For sufficiently strong amplitude and high frequency, the outcrop line velocity could be larger than the barotropic meridional one during part of the cycle, and the solution is called an entrainment solution. The annual forcing ($\omega = \omega_{\rm yr}$, $b \sim 0.2$) is an example of such a solution. For small amplitude and low frequency, however, all the subducting columns reached the permanent thermocline and the mixed layer depth could be set to a constant. This was called a nonentrainment solution. LP did not discuss which one of the two solutions was relevant to the observations. However for $b = 0.04$, which was chosen above as representative of the decadal forcing, the model response to (27) is a nonentrainment solution at periods longer than 5 years (LP, Fig. 11d). The comparison in Fig. 11 with our solution (continuous line), using for LP (dashed line) a constant mixed layer depth of 160 m clearly shows that taking into account the seasonal cycle reduces the variability by a factor of ~2, independently of the frequency since the latter is found not to affect the relation between mixed layer depth and temperature at the end of winter.

As shown in Fig. 11 by the good agreement with the dot–dashed curve, the effect of the mixed layer cycle can be parameterized by linearly relating the two variables and assuming

$$\delta d = -c\delta{\rm SST} \quad \text{with } c > 0. \tag{28}$$

Note that in all the solutions, the steepening of the interface diminishes when the period increases, as suggested above. The thermocline response to heat flux forcing becomes linear at $\omega \ll 2\pi/10$ yr.

5. Stochastic buoyancy flux forcing

As suggested by Frankignoul and Müller (1979), the sea surface density fluctuations in the midlatitudes are primarily driven by the day to day variability of the weather, which can be considered as a short timescale

→

FIG. 8. Lower-layer PV maps (normalized by f_m/H) in Apr of each year of the 10-yr modulation. The y axis is latitude and the x axis is longitude, normalized by x_w.

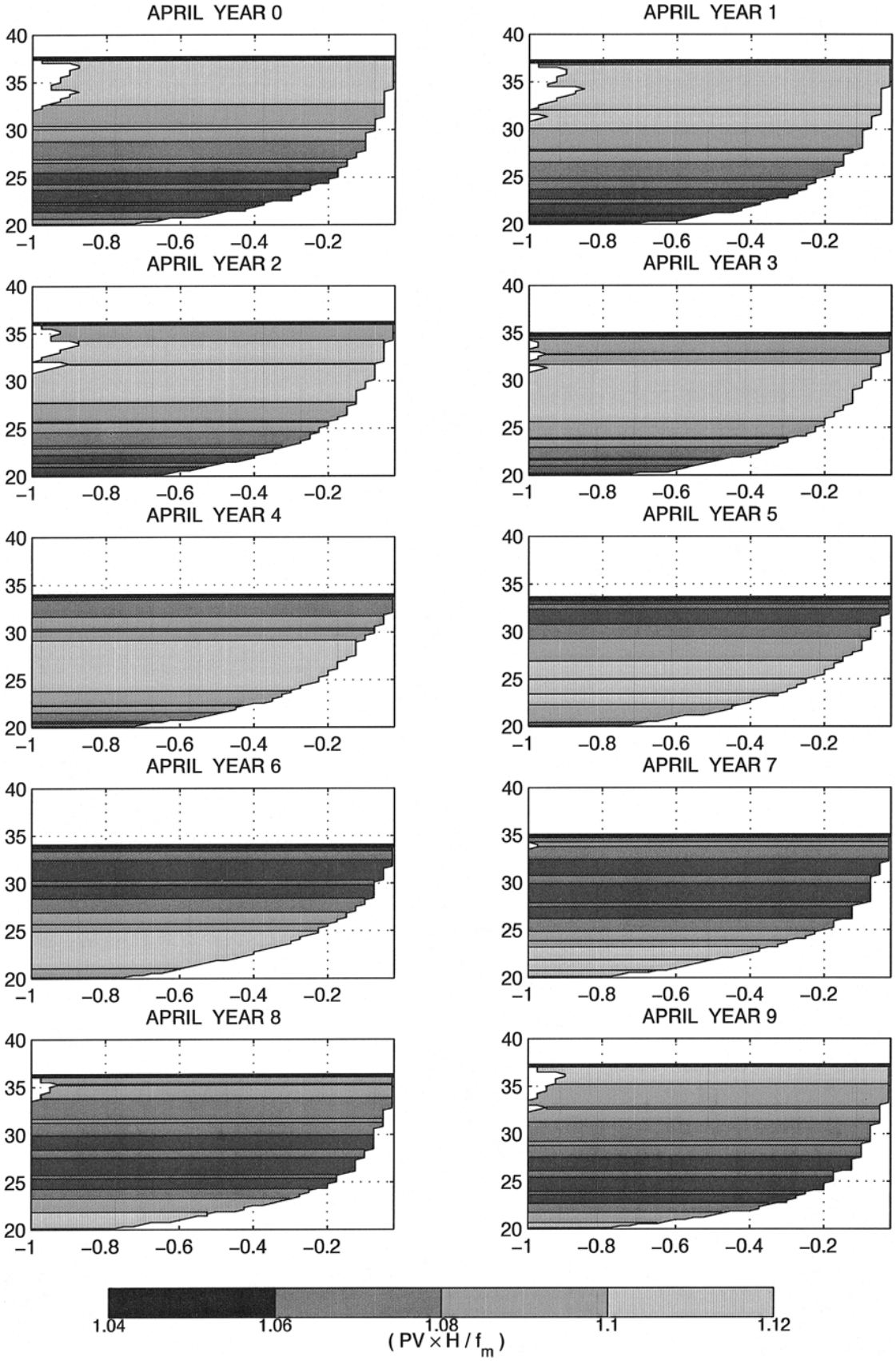
APRIL YEAR 0
APRIL YEAR 1
APRIL YEAR 2
APRIL YEAR 3
APRIL YEAR 4
APRIL YEAR 5
APRIL YEAR 6
APRIL YEAR 7
APRIL YEAR 8
APRIL YEAR 9
40
35
30
25
20
−1
−0.8
−0.6
−0.4
−0.2
1.04
1.06
1.08
1.1
1.12
(PV × H / f_m)

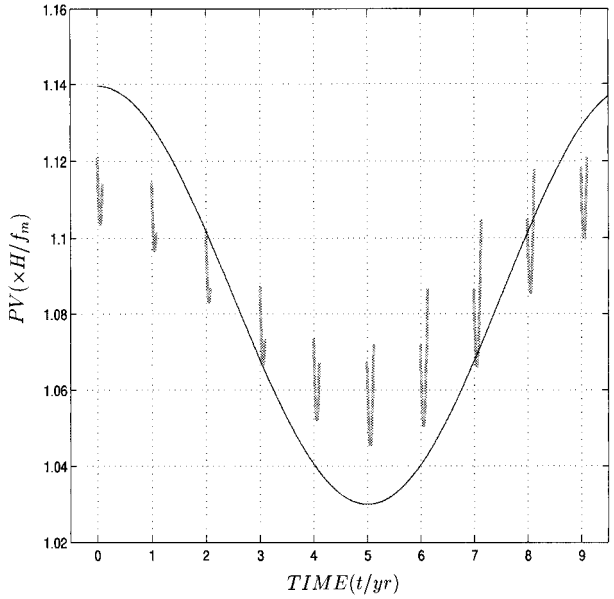

FIG. 9. Subducted PV in the permanent thermocline during each year of the 10-yr cycle (gray lines) and PV values that would be found if the mixed layer depth was always 160 m (continuous line). The PV is normalized by f_m/H.

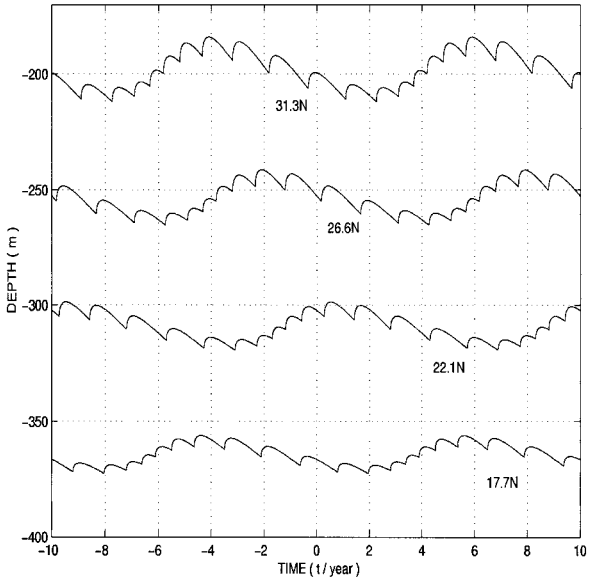

FIG. 10. Interface depth (in m) at various latitudes as a function of time for the 10-yr modulation experiment.

stochastic process. The surface buoyancy forcing of the thermocline can thus be represented as a stochastic forcing problem, which is tackled here by using the parameterization (28). We assume that the SST anomalies can be modeled by a first-order autoregressive process and neglect for simplicity the salinity effects on the density fluctuations, even though they would enhance their low-frequency variance. Then, the anomalous displacement of the outcrop line δf_{sub} is related to the SST anomaly δSST by

$$\delta\text{SST} = \frac{\mu_1}{\rho_0 \alpha_T} \delta f_{\text{sub}}, \tag{29}$$

where α_T is the thermal expansion coefficient of seawater, and (1) has been used. The dimensionless anomalous position $R_n = \delta f_{\text{sub}}/f_m(1 - a)$ of the outcrop line at the end of winter of year n is thus related to that of the previous year by

$$R_n = \alpha R_{n-1} + W_n, \tag{30}$$

where α depends on the SST anomaly persistence and W_n is a realization of a stationary white noise process. A more refined model should represent the SST anomaly evolution throughout the year and take into account their recurrence from one winter to the next (Alexander and Deser 1995) but, for the present purpose, it is sufficient to use (30) if α is representative of the year-to-year persistence of the late winter SST anomalies, which is about one year (e.g., Bhatt et al. 1998). Accordingly, the SST anomaly persistence is set to 1 yr and their variance to 0.12 K^2, which is typical of March conditions at 35°N (G. de Coëtlogon 1998, personal communication). From (28) and (29), the mixed layer depth anomaly at the end of winter in year n is $-pR_n(H - d_0)$, where d_0 is a mean mixed layer depth (160 m) and $p = \mu_1 f_m(1 - a)c/\rho_0 \alpha_T(H - d_0)$. The PV of the subducting columns at year (n) is therefore

$$q_n = \frac{f_m(1 - a)(1 + R_n)}{H - [d_0 - pR_n(H - d_0)]} = \frac{1 + R_n}{1 + pR_n} \frac{f_m(1 - a)}{H - d_0}. \tag{31}$$

The solution is computed by only following one subducted column per year, instead of tracking all the subducted columns of the effective subduction cycle of that year. Depending on the anomalous position of the outcrop line during the following years, this column may be subsequently reentrained in the mixed layer. Hence the PV spectrum in the permanent thermocline is not given by (31), but it can be computed numerically from the PV time series generated by the columns having avoided to be reentrained. Eight thousand years of integration were necessary to achieve a statistical stationary state. During the experiment, the latitude of the outcrop line at the end of winter ranges between 32°N to the subpolar gyre, for a mean position of 38°N, so for simplicity the solution is presented for latitudes lower than 32°N.

Figure 12 is a variance conserving plot of the PV in the permanent thermocline, south of 32°N. It is latitude independent since the same PV time series is obtained at each latitude, time shifted by the appropriate advective time. The variance is concentrated near the decadal frequency, and the PV anomalies have a decorrelation time of about 2 yr. The power is white at low frequencies

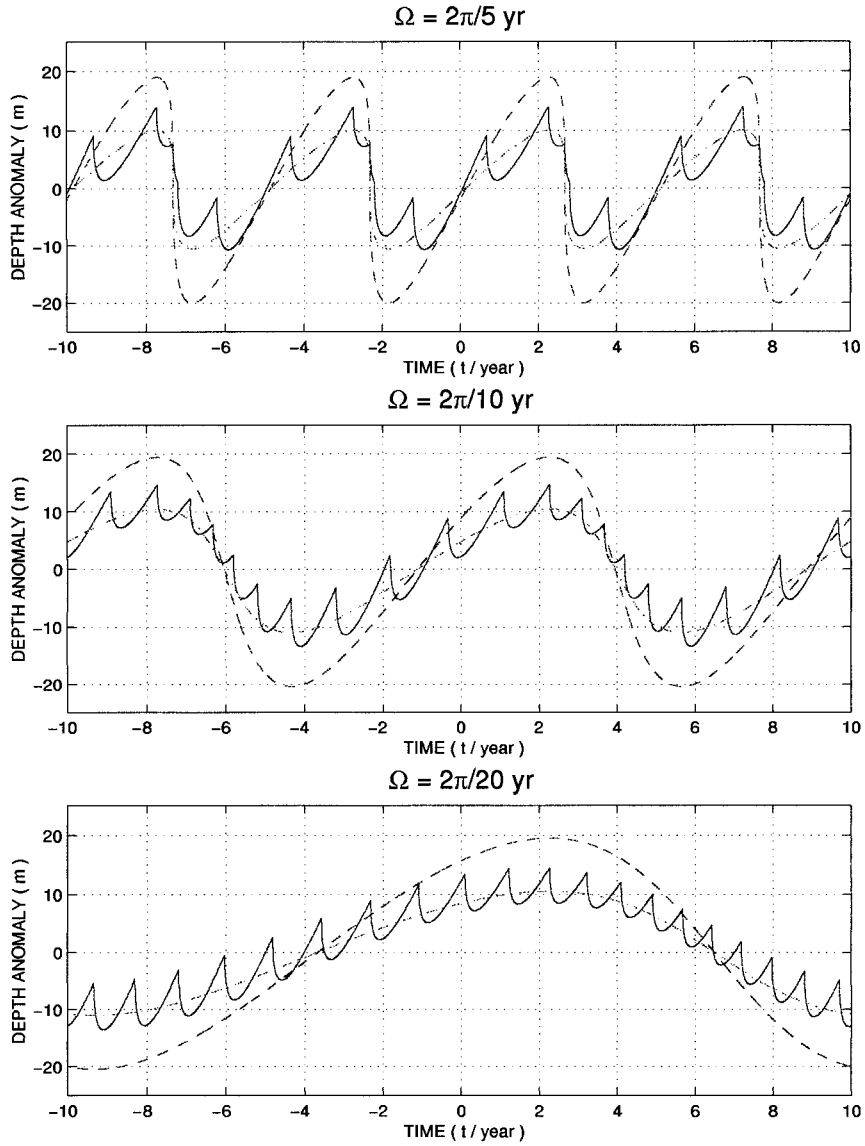

FIG. 11. Anomalies of the interface depth (in m) deduced from LP solution (dashed line) and our solution (continuous line) for various forcing frequencies but the same forcing amplitude. Top: $\omega = 2\pi/5$ yr, middle: $\omega = 2\pi/10$ yr and bottom: $\omega = 2\pi/20$ yr. Also drawn is the approximate solution (dot–dashed line) calculated with (28), using $c = 10$ m/0.5°C.

and decays approximatively as ω^{-2} at high frequencies ($\gg 2\pi/10$ yr). For comparison, the PV spectrum deduced from (31) is also plotted in Fig. 12 (dotted line). At low frequencies where the anomalous outcrop line velocity is small, subducting columns escape to be subsequently reentrained in the mixed layer (nonentrainment solution of LP) so that the two spectra are very close. This result extends to broadband forcing the frequency independence and linearity of the interior response to heat flux forcing at low frequency. Because of the assumption of a flat thermocline bottom, the interface depth is a solely function of PV, $h(f, t) = H - f/q(f, t)$, and its spectrum is very similar, except for a quadratic dependence of the power on the Coriolis parameter (note the different representation in Fig. 13). Note that the 2-yr decorrelation time of the thermocline anomalies results from two timescales. The first is associated with that of the SST anomalies, which sets the memory for q_n from one winter to the next. The second is an advective timescale set by the barotropic meridional velocity v_B and the standard deviation of the outcrop line displacement. For the standard model parameters, the two timescales are of about 1 yr and both contribute to the decorrelation time. Neglecting the SST anomaly recurrence from one winter to the next would have halved it. In corresponding simulations (not shown), the maximum variance was found

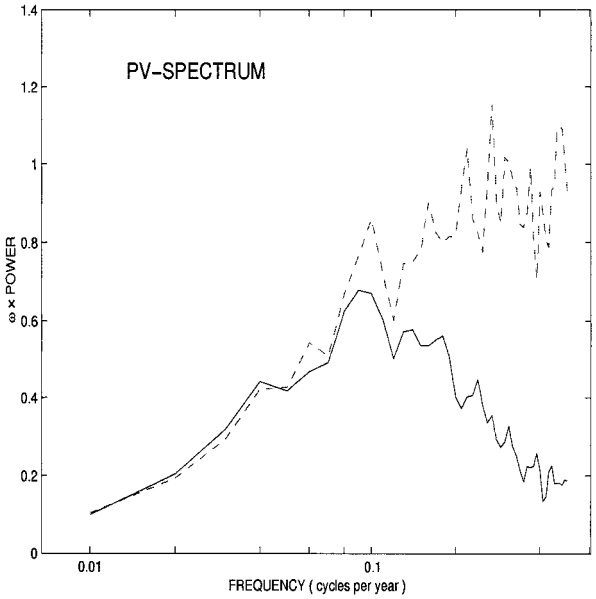

FIG. 12. Variance conserving plot of the PV spectrum in the ventilated interior (continuous line) south of 32°N, and of the spectrum based on (31) (dashed line). The spectrum is expressed in units of 10^{-4} and the PV has been normalized by $f_m(1 - a)/(H - d_0)$.

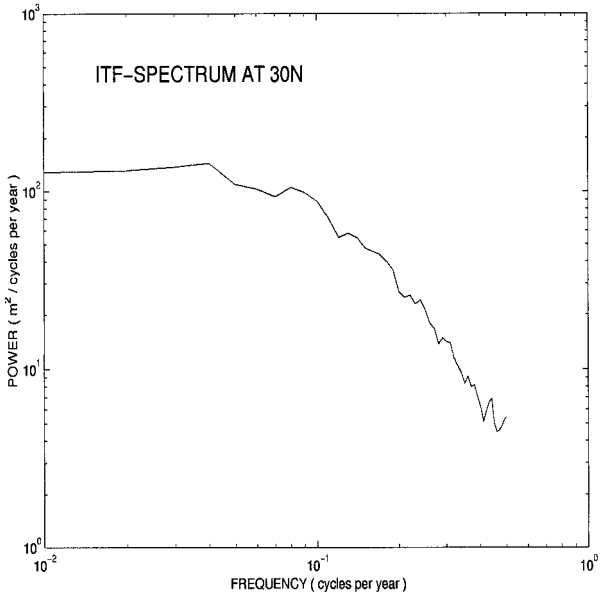

FIG. 13. Log–log plot of the interface displacement spectrum at 30°N.

indeed near the 5-yr period, as the decorrelation time would then be set by advection alone.

Since the anomalous PV at the outcrop line is correlated with the SST anomaly by (31), there is a lagged correlation between local PV or interface depth anomalies (advected downstream) and SST anomaly (latitude and longitude independent). This signature of the heat flux forcing is illustrated in Fig. 14, which shows the cross-covariance function between SST and interface depth anomalies at 30 and 20°N. A positive SST anomaly is associated downstream to a positive interface depth anomaly (positive PV anomaly) so that there is a positive peak in the cross-covariance function when SST leads the interface depth by the appropriate advective timescale (9 yr at 20°N and 3 yr at 30°N). The amplitude of the peak is smaller at 20°N because the variance of the interface depth is smaller at low latitudes.

6. Conclusions

As a simple dynamical framework to study the decadal buoyancy forcing of the subtropical gyre, we have used a two-layer planetary geostrophic model with a seasonally varying surface mixed layer. The model was forced by prescribing the displacement of the first layer outcrop line, or equivalently the sea surface density, while the surface buoyancy flux was diagnosed. The depth of the mixed layer was calculated from the prescribed outcrop line displacement, albeit in a simplified manner. Attention was restricted to the ventilated interior, where the dynamics are governed by a balance between local Ekman pumping, local thermocline response, and southward advection by the Sverdrup flow. As in LP, the mixed layer and the ventilated interior were decoupled by assuming a flat thermocline bottom and no x dependence for the mixed layer depth and density.

The model has been applied to a decadal modulation of the seasonal cycle of the mixed layer, using SST data to quantify the buoyancy forcing. The thermocline re-

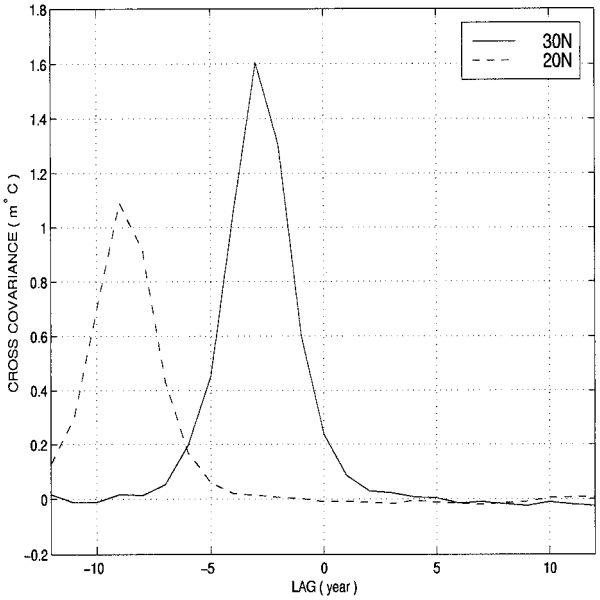

FIG. 14. Cross-covariance function between SST and interface depth anomalies (in m °C). The SST leads at negative lags.

sponse was found to be of moderate amplitude (15 m) but nonlinear, with a sharp rise and a slow decrease under harmonic modulation, which were related to periods of anomalous annual surface heat loss and gain. However, as the latter tend to zero as the period of the forcing increases, the thermocline response becomes linear at very low frequency. In the model, the decadal mixed-layer depth variations play an important role in modulating the PV of the ventilated interior because the variations of the planetary vorticity acquired by the subducting columns are of the same order as the PV anomalies induced by the mixed-layer depth fluctuations. Since they are of opposite sign, they limit the amplitude of the interior PV fluctuations, which explains why we find a thermocline variability twice smaller than in LP, who neglected the seasonal cycle and used a constant mixed layer depth.

Stochastic buoyancy forcing has also been simulated, using SST anomaly observations to specify the outcrop line displacement spectrum. Although the latter was assumed to be white for periods greater than a few years, the interior PV and interface displacement had a red spectrum, with maximum variance at decadal frequency. The cross-covariance function between interface depth and SST anomalies was furthermore predicted to peak when the latter leads the former, the time lag being simply determined by the advection of the subducted columns. These statistical signatures could be tested with sufficiently long observations or model simulations.

Unfortunately, the observations are limited. Levitus (1989) found an important rising of isopycnals in the North Atlantic between 1955–59 and 1970–74. The $\sigma_\theta = 26.5$ surface, which can be compared with the interface in the two-layer model, showed the largest signal, ranging between 150 m at the western side and 20 to 40 m at the eastern side. The latter figure is in good agreement with our prediction for a comparable SST cooling (0.5°–1°C), but there is no western intensification in our simple model. However, using a general circulation model, New and Bleck (1995) suggested that buoyancy forcing could be responsible for the larger western signal found by Levitus. Deser et al. (1996) reported that the decade-long cooling of the central Pacific between 1970 and 1991 was associated with out of phase SST and mixed-layer depth fluctuations. The ratio was typically 0.75°C/20 m, in reasonable agreement with our mixed-layer model predictions, but the subsequent isotherm displacement in the upper thermocline was about 50% larger than calculated here. However, these subducting thermal anomalies were analyzed in more details by Schneider et al. (1999), who showed that they were amplified by local forcing southward and baroclinic wave propagation associated with La Niña events. The observations may thus conform more nearly to our predictions.

A major limitation of this study is the assumption of a flat thermocline bottom, which in effect filters out the first baroclinic mode, even though Huang and Pedlosky (1999) have shown by comparing the steady-state response of more realistic models to different buoyancy forcings that the changes in the first baroclinic mode were small. A related limitation is that only barotropic meridional advection can propagate the thermocline anomalies in the ventilated zone since there can be no zonal gradient of potential vorticity, hence no Rossby waves, with a zonal outcrop line and a flat thermocline bottom. The influence of baroclinic advection should be studied by relaxing these two assumptions; the mixed layer would then be coupled with the interior circulation since anomalous geostrophic currents may alter in return the outcrop line displacement. Finally, the atmospheric forcing needs to be better represented. The assumption of a steady wind is not realistic since in reality buoyancy and mechanical forcing are coupled. Studying their joined influence on the thermocline would require a more refined mixed layer model that responds to wind mixing and a varying thermocline bottom since the first baroclinic mode is efficiently excited by Ekman pumping (Frankignoul et al. 1997).

Acknowledgments. We would like to thank Jérôme Sirven for fruitful discussions and Arthur Miller for stimulating comments. Support from the European community (ENV4-CT95-0101) is also acknowledged.

APPENDIX

Interface Depth Equation in the Ventilated Zone

Using (5) and (6), (11) can be rewritten as

$$\frac{\partial}{\partial t}\left(\frac{f}{H-h}\right) + \frac{1}{f}J\left[\gamma(\eta - h) - \gamma_m h_m, \frac{f}{H-h}\right] = 0, \tag{A1}$$

where J denotes the Jacobian, while (8) and (10) enables one to eliminate η:

$$\frac{\partial h}{\partial t} + \frac{1}{f}J\left[\frac{p_B}{\rho_0} - \frac{1}{2H}\gamma_m h_m^2,\, h\right] - \frac{\beta}{2f^2}\left(1 - \frac{h}{H}\right)\partial_x(\gamma h^2)$$

$$= -\left(1 - \frac{h}{H}\right)w_e. \tag{A2}$$

Introducing the Rossby celerity c_R, the zonal density current u_{ML} in the mixed layer, and the zonal barotropic current u_B given by

$$\begin{cases} c_R = -\beta\dfrac{\gamma h(H-h)}{Hf^2} \\ u_{\mathrm{ML}} = -\dfrac{1}{fH}\partial_y\displaystyle\int_{-h_m}^{0}\gamma_m z\,dz = \dfrac{1}{2fH}\partial_y(\gamma_m h_m^2) \\ u_B = -\dfrac{1}{f\rho_0}p_{By} = -\dfrac{x}{fH}\dfrac{d}{df}(f^2 w_e); \end{cases} \tag{A3}$$

(A2) can be rewritten as

$$\frac{\partial h}{\partial t} + (u_B + c_R + u_{\mathrm{ML}})\frac{\partial h}{\partial x} + v_B\frac{\partial h}{\partial y} = -\left(1 - \frac{h}{H}\right)w_e, \tag{A4}$$

which in characteristic form is

$$\begin{cases} \dfrac{dt}{ds} = 1 \\ \dfrac{dx}{ds} = u_B + u_{\mathrm{ML}} + c_R \\ \dfrac{df}{ds} = \dfrac{fw_e}{H} \\ \dfrac{dh}{ds} = -\left(1 - \dfrac{h}{H}\right)w_e. \end{cases} \tag{A5}$$

Here s is the distance along a characteristic curve from its initial position. The latter satisfies

$$[t, x, f, h] = [t_i, x_i, f_i, h_i] \quad \text{for } s = 0. \tag{A6}$$

The shadow zone is defined as the region covered by characteristics satisfying $[t_i, x_i, f_i, h_i] = [t_i, 0, f_i, h_E(f_i, t_i)]$ where $h_E(f, t)$ is the interface depth at the eastern boundary. Note that because the depth and density of the mixed layer are longitude independent, one has $h_E(f, t) = d(t)$ at $f = f_{\mathrm{sub}}(t)$. The recirculation zone is the region covered by characteristics satisfying $[t_i, x_i, f_i, h_i] = [t_i, x_W, f_i, h_W(f_i, t_i)]$ where $h_W(f, t)$ is the interface depth at the western boundary.

We focus our attention on the ventilated region where the characteristics originate from the outcrop line, with

$$[t_i, x_i, f_i, h_i] = [t_i, x_i, f_{\mathrm{sub}}(t_i), d(t_i)]. \tag{A7}$$

Two equations can be derived from (A5). First, since

$$\frac{dq}{ds} = \frac{1}{H - h}\frac{df}{ds} + \frac{f}{(H - h)^2}\frac{dh}{ds} = 0, \tag{A8}$$

PV is conserved following the characteristic,

$$\frac{f}{H - h} = \frac{f_i}{H - h_i}. \tag{A9}$$

Second, rewriting the second line of (A5) as

$$\frac{dx}{ds} = \frac{dx}{df}\frac{f}{H}w_e = \frac{-x}{fH}\frac{d}{df}(f^2w_e) - \beta\gamma\frac{h(H - h)}{f^2H} + \frac{\beta}{fH}\frac{d}{df}\left(\frac{1}{2}\gamma_m h_m^2\right), \tag{A10}$$

where we have used (A3), and integrating along the characteristic of initial condition $[t_i, x_i, f_i, h_i]$, we find after some algebra

$$xf^2w_e(f) = x_i f_i^2 w_e(f_i) + \beta\left[\frac{1}{2}\gamma(h^2 - h_i^2) + \frac{1}{2}\gamma_m(f)h_m^2(f) - \frac{1}{2}\gamma_m(f_i)h_m^2(f_i)\right]. \tag{A11}$$

The values of f and h propagated by each characteristics only depend on t_i since, from (A5) and (A7), $df/ds = w_e = w_e(f)$ and $h = H[1 - f/f_{\mathrm{sub}}(t_i)(1 - d(t_i)/H)]$. Characteristics with a different x_i ($x_i \in [x_W 0]$) propagate, therefore, a similar value of h and f, but they reach a different longitude in view of (A11). The easternmost characteristics emanating from the outcrop line verify $[t_i, x_i, f_i, h_i] = [t_i, 0, f_{\mathrm{sub}}(t_i), d(t_i)]$ and define the boundary $x_{\mathrm{SZ}}(f, t)$ with the shadow zone, satisfying

$$x_{\mathrm{SZ}}f^2w_e(f) = \frac{\beta}{2}[\gamma(h^2 - h_i^2) + \gamma_m(f)h_m^2(f) - \gamma_m(f_i)h_m^2(f_i)]. \tag{A12}$$

The westernmost characteristics emanating from the outcrop line verify $[t_i, x_i, f_i, h_i] = [t_i, x_W, f_{\mathrm{sub}}(t_i), d(t_i)]$ and define the boundary $x_{\mathrm{RZ}}(f, t)$ between the recirculation and the ventilated zone, satisfying

$$x_{\mathrm{RZ}}f^2w_e(f) = x_{\mathrm{SZ}}f^2w_e(f) + x_W f_i^2 w_e(f_i). \tag{A13}$$

Between $x_{\mathrm{SZ}}(f, t)$ and $x_{\mathrm{RZ}}(f, t)$, the solution is longitude independent.

REFERENCES

Alexander, M. A., and C. Deser, 1995: A mechanism for the recurrence of wintertime midlatitude SST anomalies. *J. Phys. Oceanogr.*, **25,** 122–137.

Bhatt, U. S., M. A. Alexander, D. S. Battisti, D. D. Houghton, and L. M. Keller, 1998: Atmosphere–ocean interaction in the North Atlantic: Near-surface climate variability. *J. Climate*, **11,** 1615–1632.

Deser, C., M. A. Alexander, and M. S. Timlin, 1996: Upper ocean thermal variations in the North Pacific during 1970–1991. *J. Phys. Oceanogr.*, **26,** 1840–1855.

Frankignoul, C., and P. Müller, 1979: On the generation of geostrophic eddies by surface buoyancy flux anomalies. *J. Phys. Oceanogr.*, **9,** 1207–1213.

——, ——, and E. Zorita, 1997: A simple model of the decadal response of the ocean to stochastic wind forcing. *J. Phys. Oceanogr.*, **27,** 1533–1546.

Huang, R. X., and J. Pedlosky, 1999: Climate variability inferred from a layered model of the ventilated thermocline. *J. Phys. Oceanogr.*, **29,** 779–790.

Levitus, S., 1982: *Climatological Atlas of the World Ocean.* NOAA Prof. Paper No. 13, U.S. Govt. Printing Office, 173 pp.

——, 1989: Interpendental variability of temperature and salinity at intermediate depth of the North Atlantic Ocean, 1970–1974 versus 1955–1959. *J. Geophys. Res.*, **94,** 6091–6131.

Liu, Z., and J. Pedlosky, 1994: Thermocline forced by annual and surface surface temperature variations. *J. Phys. Oceanogr.*, **24,** 587–608.

Marshall, J. C., A. J. G. Nurser, and R. G. Williams, 1993: Inferring the subduction rate and period over the North Atlantic. *J. Phys. Oceanogr.*, **23,** 1315–1329.

Miller, A. J., D. R. Cayan, T. P. Barnett, N. E. Graham, and J. M. Oberhuber, 1994: Interdecadal variability of the Pacific Ocean:

Model response to observed heat flux and wind stress anomalies. *Climate Dyn.,* **9,** 287–302.

New, A. L., and R. Bleck, 1995: An isopycnic model study of the North Atlantic. Part II: Interdecadal variability of the subtropical gyre. *J. Phys. Oceanogr.,* **25,** 2700–2714.

Paillet, J., and M. Arhan, 1996: Shallow pycnoclines and mode water subduction in the eastern North Atlantic. *J. Phys. Oceanogr.*, **26,** 96–114.

Schneider, N., A. J. Miller, M. A. Alexander, and C. Deser, 1999: Subduction of decadal North Pacific temperature anomalies: Observations and dynamics. *J. Phys. Oceanogr.,* **29,** 1056–1070.

Stommel, H., 1979: Determination of water-mass properties of water pumped down from the Ekman-layer to the geostrophic flow below. *Proc. Natl. Acad. Sci. USA,* **76,** 3051–3055.

Williams, R. G., M. A. Spall, and J. C. Marshall, 1995: Does Stommel's mixed layer demon work? *J. Phys. Oceanogr.,* **25,** 3089–3102.